ELSEVIER

Chemical Engineering Journal 140 (2008) 539–554

Chemical Engineering Journal

www.elsevier.com/locate/cej

Evaluation of downer reactor performance by catalytic ozone decomposition

Chuigang Fan [a,b], Yong Zhang [d], Xiaotao Bi [c], Wenli Song [a,*], Weigang Lin [a], Ling'ai Luo [e]

[a] *Multi-phase Reaction Laboratory, Institute of Process Engineering, Chinese Academy of Sciences, Beijing 100080, PR China*

[b] *Graduate School of Chinese Academy of Sciences, Beijing 100049, PR China*

[c] *Fluidization Research Centre, University of British Columbia, Vancouver, Canada*

[d] *China Huan-Qiu Contracting & Engineering Corporation (HQCEC), Beijing, PR China*

[e] *Université de Savoie, France*

Received 11 September 2007; received in revised form 30 November 2007; accepted 30 November 2007

Abstract

Radial distribution profiles of ozone concentrations were measured along an 8.50 m high and 0.09 m inside diameter gas/solid co-current downflow circulating fluidized bed (downer) to characterize the reactor performance. Tests were conducted under a series of operating conditions at room temperature and near atmospheric pressure, with FCC particles as the bed material. Results show that the concentration distribution of the ozone tracer gas correlates well with the flow structure of the downer. There is quite a uniform radial distribution of ozone concentrations in the core region of all tested axial sections in the fully developed region of the downer, except for the near-wall region where there is a sharp decrease in ozone concentration. And there exists a relatively significant non-uniform distribution in the entrance acceleration region of the downer.

Keywords: Downer; Mass transfer; Ozone decomposition; Fluidization; Circulating fluidized bed; Cluster

1. Introduction

Although CFB-riser reactors have shown many advantages over conventional bubbling fluidized bed reactors such as high gas/solids contacting efficiency, reduced axial dispersion of both gas and solids phases, and high gas solids throughput, etc., it suffers from severe solids back-mixing due to non-uniform gas and solids flowing against gravity. The core/annulus structure can result in reduced contacting between the two phases, causing reduced selectivity and non-uniform distribution of desired product [1].

For heterogeneous catalytic reactions the conversion of reactant to the desired product is accompanied by consecutive and/or side reactions, which lead to a decrease in selectivity and yield. Such reactions require a reactor with a narrow residence time distribution for both the gas and solid phases in order to achieve satisfactory reaction control [2,3].

In recent years, a novel reactor called the downer, with both gas and solid particles moving in the direction of gravity – a type of generalized fluidization [4] – has been proposed, which can overcome those shortcomings of the riser as mentioned before. The gas and solids downwards flow in the downer can reduce the non-uniformities of flow, making the flow in the downer much closer to plug flow than in the riser, so that much narrower residence time distribution of gas and particles can be achieved. The downer is an excellent choice for reactions requiring very short residence time especially where intermediates are the desired products [5,6].

Much fundamental research has been carried out on the hydrodynamic characteristics of the downer, but few results have been reported on heat and mass transfer or chemical reactions [7,8] as compared to hydrodynamic studies. A clear understanding of heat/mass transfer and chemical reactions in the downer will help in the design of downer reactors.

There has been no previous study that provides overall and systematic reactant concentration distribution profiles inside a downer. When studying a chemical reactor, chemical reaction itself can supply direct information on reactor performance.

* Corresponding author. Tel.: +86 10 82627075.
E-mail address: wlsong@home.ipe.ac.cn (W. Song).

1385-8947/$ – see front matter © 2007 Elsevier B.V. All rights reserved.
doi:10.1016/j.cej.2007.11.040

Nomenclature

Nomenclature

A_b	cross section area of downer [m^2]
c_i (i = 1,2,s,0)	average ozone concentration, see Eq. (3)
C/C_0	dimensionless ozone concentration
d_p	particle diameter [μm]
D_g	dispersion coefficient of ozone [m^2/s]
G_s	solids circulation rate [kg/m^2 s]
k	reaction rate constant [ml/(gcat s)]
k_g	mass transfer coefficient [m/s]
r/R	dimensionless radial position
Re	Reynolds number.
Sc	Schmidt number
Sh	Sherwood number
u_s	slip velocity [m/s]
U_g	superficial gas velocity [m/s]
z	axial distance from the gas distributor of downer [m]
z/H	dimensionless axial position

Greek letters

ε	bed voidage
φ	angular position for measurement [°]
ν	kinematic viscosity [m^2/s]
ρ_p	particle density [kg/m^3]

Because of its simplicity in reaction kinetics (very close to first-order reaction) and negligible heat effect of reaction due to the low concentrations involved, and the availability of a simple and accurate measurement method, in the present study, a heterogeneous catalytic reaction which is often used in research on dense fluidized beds and CFB riser reactors [9–16] – ozone decomposition catalyzed by ferric oxide – was employed to investigate reaction coupled to mass transfer in a downer reactor.

In the present paper, experimental data of radial ozone concentration profiles at different axial locations along a downer reactor are reported under a series of operating conditions. The influences of operating conditions on reactor performance as measured at different radial/axial positions were analyzed.

2. Experimental details

2.1. The downer reactor system

The experimental apparatus used in this study is depicted in Fig. 1. All measurements were conducted in a circulating fluidized bed downer reactor of 8.50 m high with an inside diameter of 0.09 m. The whole setup is made of Plexiglas. Solids are transported upward in the riser, and then separated from the exhaust by two cyclones before being returned to a storage tank above the downer column. Solids enter the downer via a butterfly valve. Air from a screw air compressor is used as the fluidizing gas for the whole experimental system (main air, lift air and auxiliary air). The air is first introduced into a compressed air freezing dryer and a filter system in order to maintain a constant relative

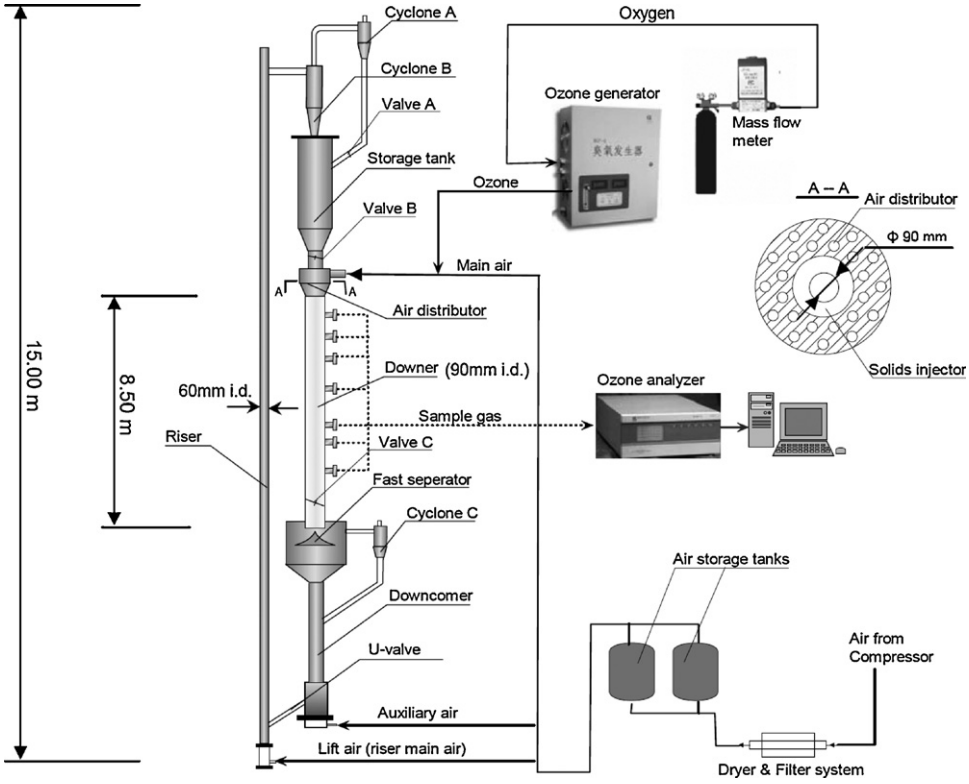

Fig. 1. Schematic of the downer reactor and ozone injection and detection system.

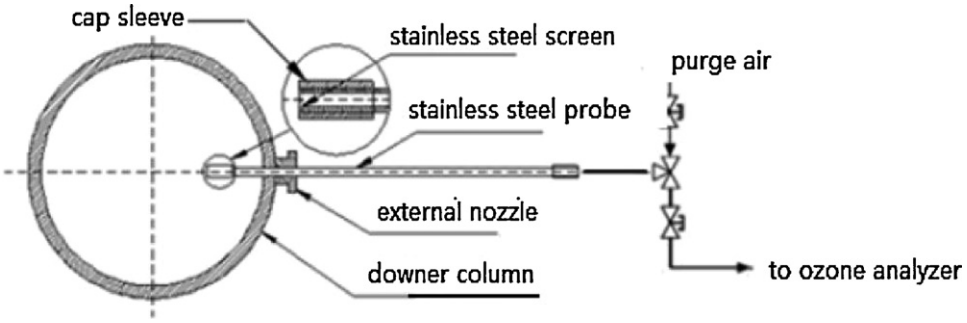

Fig. 2. Sampling system for ozone concentration measurements.

humidity. The main air is introduced at the distribution plate. The gas/solids suspension travels downward along the downer to an elaborately designed quick separator [17] located at the bottom of the downer column in order to separate the particles from the air. Solids separated from the gas are then returned to the riser via a U-valve.

Ozone is generated from a corona-discharge generator connected to the main air supply system. Pure oxygen is used as the source of ozone in order to eliminate the formation of harmful NO_x during the electrical discharge process [9,18,19]. Ozone from the generator was completely mixed with the primary air before entering the downer above the gas distributor. The current and voltage of the ozone generator as well as the temperature and relative humidity are all monitored during each measurement.

All pressure differences around the loop were monitored with open-end water-filled manometers, and the axial distribution of cross-sectional voidage in the downer can be calculated from the measured pressure gradient. The pressures are measured at 8 levels below the air distributor along the downer (i.e., 81.8, 181.7, 202.7, 302.7, 403.7, 504.7, 606.7 and 767.7 cm).

A UV detection system is used to measure the ozone concentration, as described elsewhere [9,11]. To obtain radial and axial ozone concentration profiles, laterally movable sampling probes are installed at axial distances of 1.00, 2.57, 3.51, 4.51 and 6.51 m from the gas distributor. Gas samples are continuously drawn from the downer through a sampling system shown in Fig. 2, using the stainless steel or quartz glass sampling probes with a length of 135–140 mm and an inside diameter of approximately 2 mm. The tip of the probe is covered with a fine mesh to prevent particles from being entrained into the sampling system. The sample gas flow rate is low enough to assure minimal disturbance of the flow structure in the downer. Each probe is flushed with purge air before measurement. Because ozone is a strong oxidizing agent and reacts with practically any reducing organic or inorganic agent, undesirable decomposition of ozone was minimized by using silicone, glass and Teflon tubings for all connections.

Measurement was started after steady state had been reached in the downer reactor, which usually took about 1.5–2.5 h [18]. Before tests, the inlet oxygen flow to the ozone generator and the mass flow meter were calibrated to determine the inlet ozone concentration of the downer reactor.

2.2. Operating conditions

The gas flow in the downer is denoted as the superficial gas velocity of U_g, and the value of G_s (solids circulation rate) is controlled by the gas flow rate in the riser. The determination of G_s was accomplished by a butterfly valve fixed in the downer column. When the valve closes rapidly, particles will accumulate to a specific height above the valve over a given time period. Hence, once the bulk density of the particles and the cross-section area of the downer column are known, the solids circulation rates can be calculated from the solids height. In each test, this operation was repeated several times to obtain an average value, such as those shown in Fig. 3.

The selection of G_s is based on the lift capacity of the riser. As illustrated in Fig. 4, the lift capacity is reached with the increase of the air flow rate in the riser to a certain value.

The experimental operating conditions are given in Tables 1 and 2.

2.3. Experiment for determining reaction rate constant

Besides the experiments conducted in the CFB-downer reactor, the measurement of reaction rate constant of ozone decomposition catalyzed by the ferric oxide was conducted in a small scale fixed bed reactor system as shown in Fig. 5.

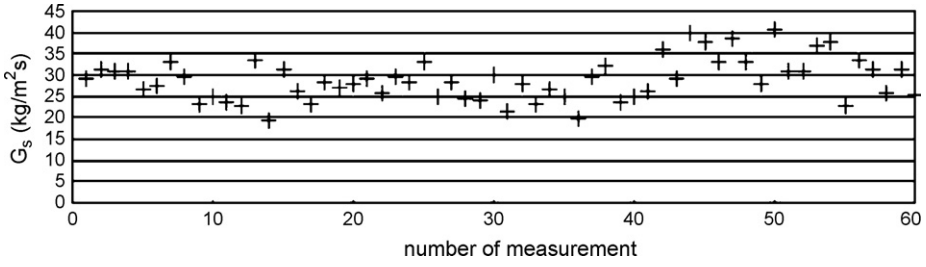

Fig. 3. Part of the data in a G_s (kg/m^2 s) determination test.

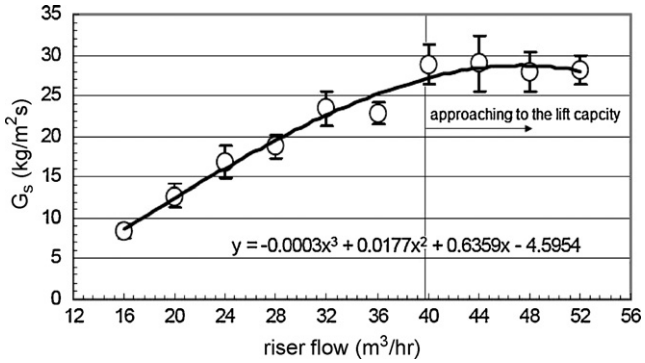

Fig. 4. Determination of the range of G_s.

Table 1
Operating conditions of the experiment (stainless steel probe) (U_g: m/s; G_s: kg/m^2 s)

U_g	G_s					
	2.36	2.77	3.35	6.58	9.1	10.4
2.49	–			–		
2.84			–		–	
3.07		–				–

Table 2
Operating conditions of the experiment [quartz glass probe]

Q_{riser}(m^3/h)	16	20	24	26	32	40
G_s (kg/m^2 s)	8.4	12.7	16.9	18.7	23.4	28.8
Q_{downer} (m^3/h)	50	60	70	80	65	
U_g (m/s)	2.2	2.6	3.1	3.5	3.7	

Size and structure of the quartz glass probes are identical to stainless steel probes.

The small fixed bed reactor is made of stainless steel, with an inside diameter of 20 mm and a bed length of 70 mm. The fixed bed of catalyst powder is supported by a stainless steel mesh screen covered with canvas. Both inlet and outlet are screwed with stainless steel nipples for connection to gas flow tubings. The ozone concentration was determined volumetrically by iodimetry according to the following reactions.

$$O_3 + 2KI + H_2O = O_2 + I_2 + 2KOH$$

$$I_2 + 2Na_2S_2O_3 = 2NaI + Na_2S_4O_6.$$

The ozone conversion data from the fixed bed reactor were used to extract the reaction rate constant of catalytic ozone decomposition after the effect of external/internal diffusion and fixed bed wall on the reaction process had been eliminated. The average reaction rate constant obtained from this measurement was 0.098 ml (g cat)$^{-1}$ s^{-1}, and this value was later used in the computation for analyzing the ozone decomposition data obtained from the downer reactor. Further details of the kinetics measurement are given in Appendix A.

2.4. Catalyst preparation

The catalyst used in the experiments was equilibrium fluid cracking catalyst (FCC) particles (composed mainly of porous amorphous aluminum hydro-silicate) impregnated with ferric oxides. The FCC particles were activated by soaking in a 5 wt.% solution of ferric nitrate overnight, followed by drying, and calcination at 475 °C for about 2 h until no NO_2 was released from ferric nitrate, and then the remaining ferric oxide became the active component for ozone decomposition.

$$\left(Fe(NO_3)_3 \cdot nH_2O \xrightarrow{\geq 370\,^\circ C} \frac{1}{2}Fe_2O_3 + 3NO_2 + \frac{3}{4}O_2 + nH_2O\right)$$

An elemental analysis of the catalyst particle was performed for both the fresh FCC particles and the activated FCC particles. The bulk density of the particles without/with ferric oxide impregnation is 585 and 755 kg/m^3, respectively. The apparent particle density is 1400 kg/m^3, and 1747 kg/m^3 for fresh FCC and impregnated FCC particles, respectively. The mean diameter of fresh FCC particles is 72 μm, which changed to 62 μm after being impregnated with ferric oxide and followed by grinding.

3. Experimental results and discussion

3.1. Radial profiles of ozone concentration in the downer

In order to observe whether there is a large amount of ozone decomposition caused by the wall of the reactor and the catalytic performance of ferric oxide in a downer reactor, experiments were first conducted in the empty downer column (Fig. 6a), and then with the fresh FCC particles (Fig. 6b), and finally with ferric oxide impregnated FCC particles (Fig. 6c) by measuring the radial profiles of ozone concentration at different axial positions

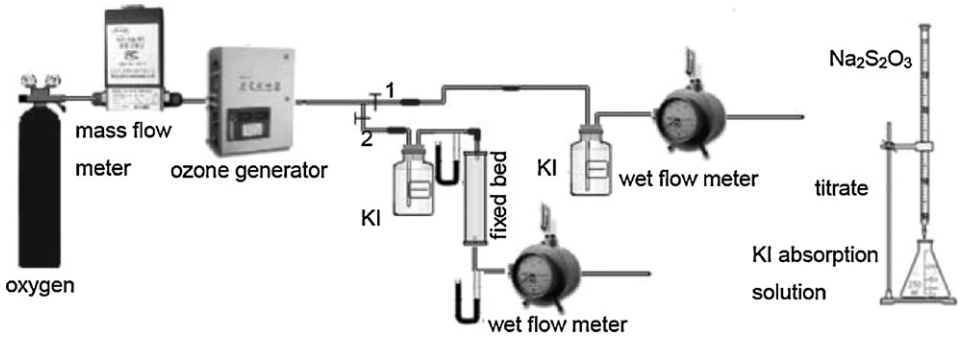

Fig. 5. Flow sheet of the fixed bed test unit.

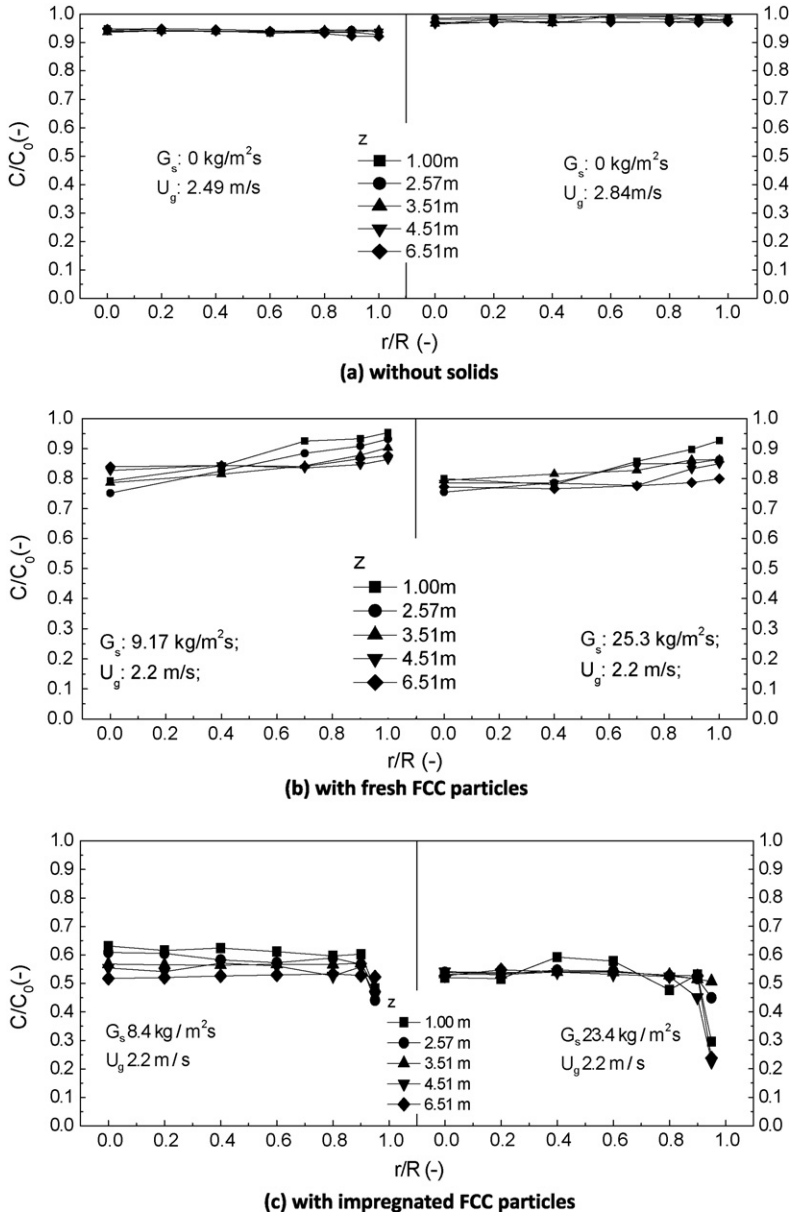

Fig. 6. Radial ozone concentration profiles comparison.

each at the following $r/R = 0$, 0.2, 0.3, 0.4 0.6, 0.8, 0.9 and 0.95 radial positions (the ozone concentration cannot be obtained reliably when the probe is exactly placed at $r/R = 1$).

By comparing Fig. 6a with c, it can be seen that unconverted ozone concentration in a is much higher than that in c, indicating that ozone decomposition caused by the reactor wall is much less than that caused by the catalyst.

Fig. 7 shows that there is essentially little decomposition of ozone in the empty downer column, the ozone concentration in the empty downer remaining as high as 90% of the inlet concentration, as compared to 40–60% after catalyst is fed into the reactor.

Comparison between Fig. 6c and b reveals that ferric oxide reduces the ozone concentration particularly from $C/C_0 = 0.8$–0.9 (Fig. 6b) to $C/C_0 = 0.5$–0.6 (Fig. 6c) under similar operating conditions with the profile at the core region of downer remaining as flat as in Fig. 6b, and at $r/R = 0.8$–0.9, reaching a minimum at about $r/R = 0.95$.

Such a sharp drop in ozone concentration near the wall is not obvious in Fig. 6a and b, evidently due to heterogeneous flow structure in downers with more catalyst concentrating in the near wall region. In the fully developed region of the downer particles tend to move towards the wall ($r/R = 0.9$–1) and form many clusters (meso-scale structures), which has been testified by the hydrodynamics study performed in the same downer reactor by Li [20] and many prior researchers' work on the downer [21,22]. In the present study, with activated catalyst particles employed, the existence of a densely populated "active clusters" region (or active dense phase) at $r/R = 0.9$–1 increases ozone decomposition, leading to the increase of reactant conversion [12] and

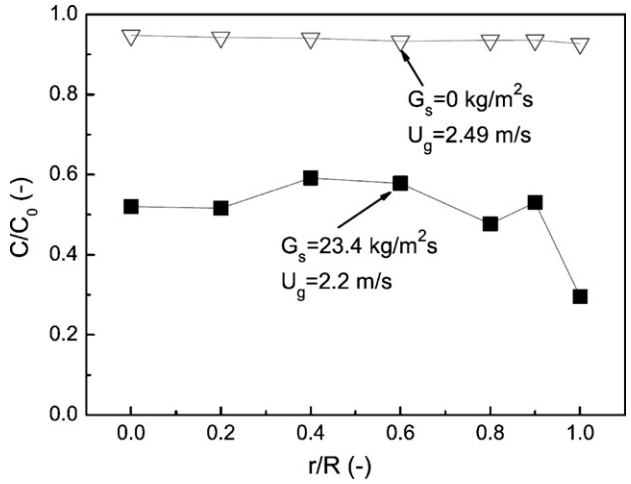

Fig. 7. Ozone concentration profiles at the inlet region of the downer ($z = 1.00$ m) for both empty column and column loaded with impregnated catalyst particles.

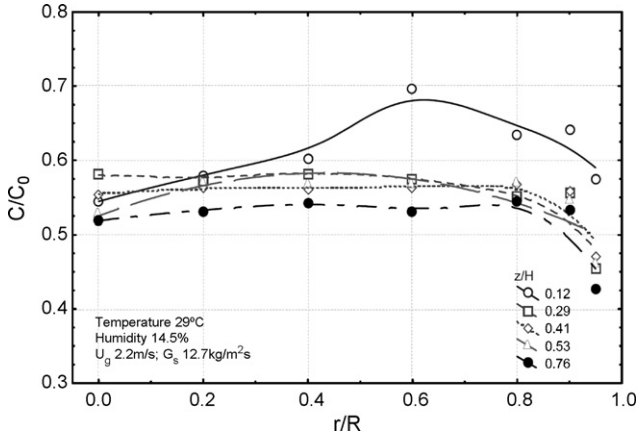

Fig. 9. Typical radial ozone profiles at different axial levels in the downer.

faster reaction rates [23], thus lowering ozone concentration at the near-wall region.

Rotational asymmetry of ozone concentration distribution in the entrance region of the downer was also investigated before each run. The radial ozone profiles at $z = 1.00$ m had been measured along 4 different angular positions ($\varphi = 0$–$270°$) for 3 times under the same operating condition and similar rotational asymmetry were observed. Fig. 8a shows a representative result. The profiles from 4 measurements exhibit significant differences: the ozone concentration profile measured along $\varphi = 0°$ and 270° is significantly lower than that at $\varphi = 90°$ and 180°. In the earlier experiment at the same axial position, ozone was sampled along the angular position of $\varphi = 270°$, which is located in the low-concentration region. Therefore, the measured concentration is lower than the cross-sectional averaged value. So it is better to average the ozone concentration data measured along 4 angular positions to get a more accurate profile. Furthermore, tests performed in the fully developed region of the downer (see Fig. 8b) show that radial profiles are as flat as earlier measurements, which means that the asymmetry is insignificant in fully developed region, and the previous measurements are of representative nature. Hence, there is no need to make measurements along 4 angular directions for the measurements in the fully developed region.

In consideration of the rotational asymmetry of the ozone concentration in the entrance region of the downer, radial concentration measurements at this region were repeated along four angular directions, and the averaged values were used as the cross-sectional average concentration at this axial location (a typical and clearer view is depicted in Fig. 9). This is a common and effective procedure for minimizing the influence of rotational asymmetry on the measurements and has been successfully employed by many researchers, such as Kruse and Werther [24] and Ouyang et al. [14] (data at $z/H = 0.12$ were averaged over four different radial directions).

3.2. Influence of operating conditions on ozone distribution and conversion

Thirty runs of systematic measurements were performed under the operating conditions given in Table 2. The ozone concentration profiles at $z = 1.00$ m ($z/H = 0.12$) were obtained from the averaged method mentioned before, with the results shown in Fig. 10. As a general trend, the unconverted ozone concentration is seen to increase with increasing U_g and decreasing G_s. In addition, the decrease of ozone concentration near the wall seems to be sharper as U_g and G_s increase.

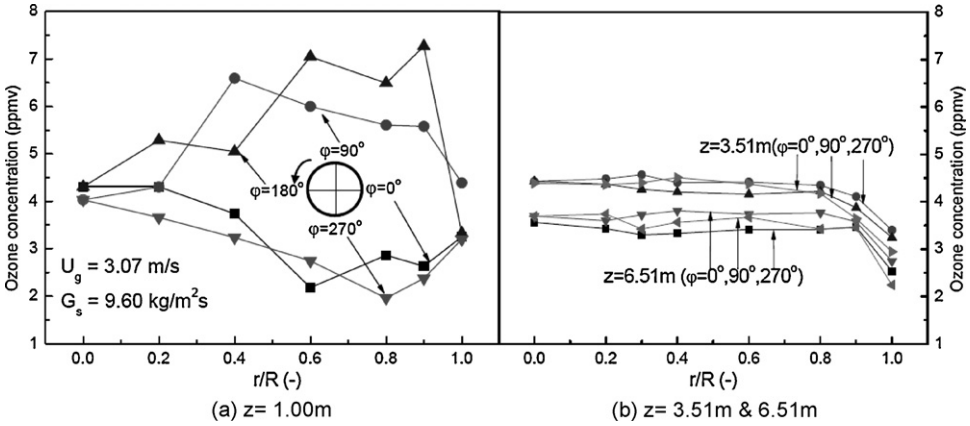

Fig. 8. Rotational asymmetry at the inlet region of the downer column.

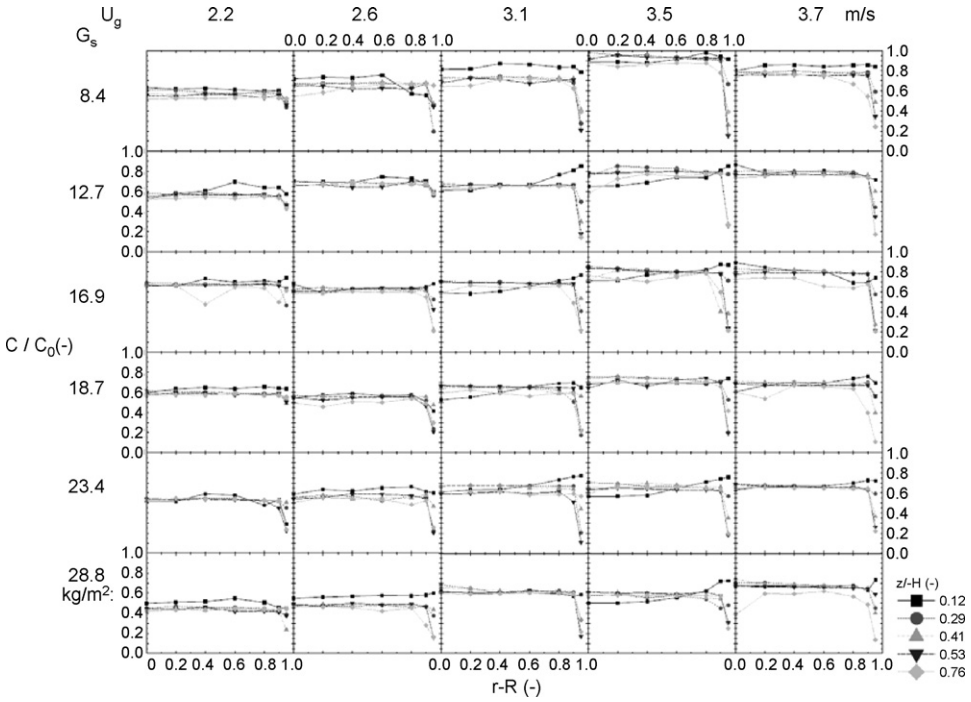

Fig. 10. Ozone decomposition in downer under different operating conditions (quartz glass tube in use).

The large amount of data in Fig. 10 could hardly be discriminated from each other. For a clearer view on the data set, the scattered raw data of the experiment were re-plotted according to the classification of ozone concentration distribution at different axial locations under different value of U_g for the same value of G_s (Fig. 11a and b) or under different G_s for the same U_g (Fig. 12a and b). Additional figures are provided in Appendices B and C. The radial distributions of ozone concentration illustrated from Fig. 11a and b are similar to those in Fig. 6c, i.e., a flat distribution exists in the core region and a sharp drop appears near the reactor wall. The results are fairly reproducible.

It can be seen from Fig. 11a and b and Appendix B that the concentration of the unconverted ozone increases with increasing the superficial gas velocity at a given solids circulation rate (especially at a high G_s), while it is seen from Fig. 12a and b that the unconverted ozone concentration decreases with increasing solids circulation rate at a given superficial gas velocity (especially at a high gas velocity). This may be attributed to the following mechanisms.

When the solids flux is increased at a given superficial gas velocity, the solids concentration will also increase. Due to the increase of total gas/solids contact area for gas/solids mass transfer and reaction, the ozone conversion is increased, leading to lower unconverted ozone concentration as the solids circulating rate increases.

The effect of solids circulation rate is more significant at a higher superficial gas velocity (Fig. 12b) than at a lower superficial gas velocity (Fig. 12a). This is because at a low superficial gas velocity, the increase of solids concentration can lead to increased formation probability of particle clusters in addition to increased gas/solid contact area. The clusters will be formed easily at a relatively low gas velocity as the solids circulating rate is increased, and the gas/solid mass transfer within the clusters is not as good as that between dispersed particles and surrounding gas. On the other hand, the formation of the clusters results in increased slip velocity between the gas and solid phases, which improves the inter-phase mass transfer. The compromise of all those counter-acting factors invites the relatively obscured trends in the radial ozone concentration profiles at low superficial gas velocities. This is also confirmed from the calculated axial ozone conversion profile to be discussed later.

When the solids circulation rate is kept invariant, increasing superficial gas velocity can reduce solids concentration, breaking down the clusters, increasing the slip velocity between the gas and particles, and shortening the residence time of the solids phase. The decreased solids concentration and clusters breakdown rate can decrease total gas/solids contact area and improve local gas/solids contact efficiency, respectively, at the same time. The increase of slip velocity will enhance the mass transfer rate between the gas and solids. The shortened residence time is not good for the total conversion of ozone, especially when the flow direction of gas/solid suspension is downward. Taking into consideration all of the above-mentioned factors, the increase of superficial gas velocity may finally lead to the fall of ozone conversion for a fast catalytic reaction in a gas/solids concurrent down-flowing reactor in spite of the improvement in local mass transfer.

The ozone concentration drop near the wall ($r/R = 0.9$–0.97) is generally more significant under higher superficial gas velocities than that under lower superficial gas velocities at a given solids circulating rate (Fig. 11a and b and Appendix B). But this tendency is not very obvious with increasing solids circulating rate under a specific superficial gas velocity (Fig. 12a and b and Appendix C).

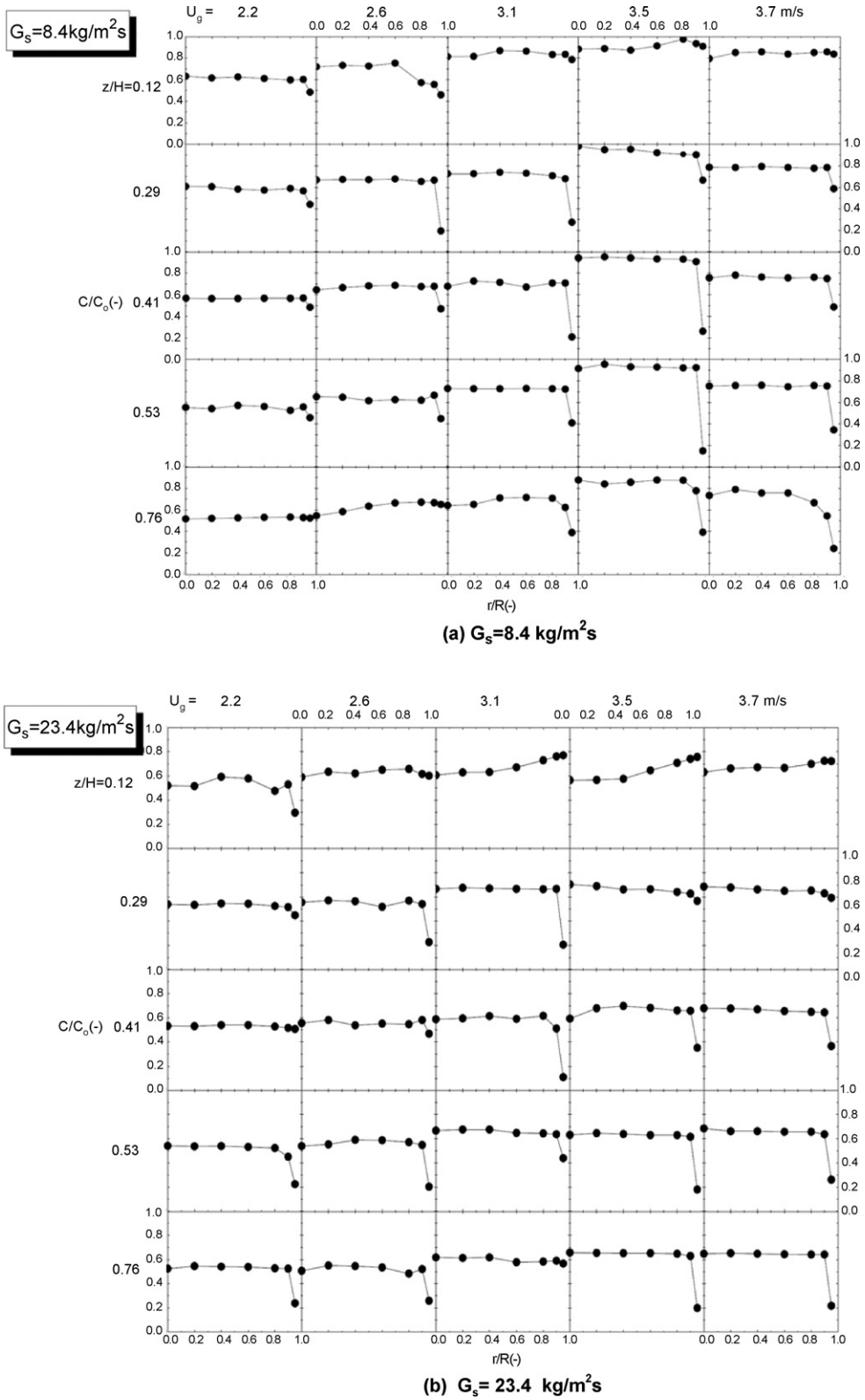

Fig. 11. Ozone concentration distribution for different values of U_g.

The trend in Fig. 12a and b may also be the result of the compromise of several counter-acting factors similar to those discussed above. The cluster plays a key role in accounting for the phenomenon at this narrow wall region. In brief, for the former case, the clusters near the wall are easier to be broken by gas flow (i.e. a higher frequency of aggregation–dispersion process of particles) when the gas velocity is increased and the slip velocity between the gas and dispersed particles is also

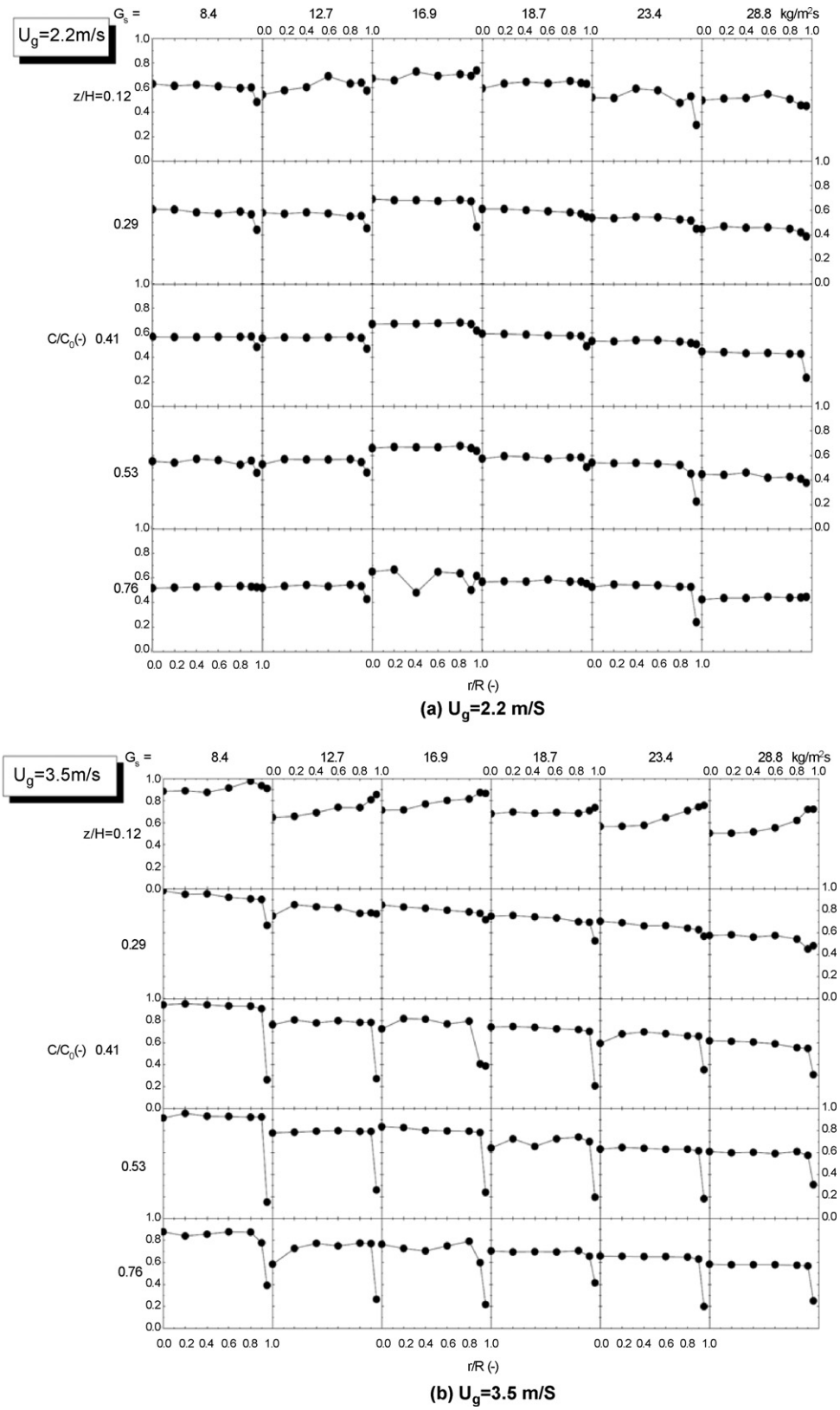

Fig. 12. Ozone concentration distribution for different values of G_s.

increased simultaneously, with both factors being beneficial for the improvement of gas/solids mass transfer at this region; but for the latter case, the solids concentration will be increased with increasing the solids circulation rate under a fixed superficial gas velocity, hence more clusters may be easily formed, leading to the enhancement of shielding effect between the clusters and an increase of slip velocity between clusters and gas flow simultaneously. It can be concluded (from Fig. 11 and Appendix B)

that the compromise of the two opposite factors leads to the ozone conversion at the near-wall region being insensitive to the variation of solids flux under a fixed superficial gas velocity.

Figs. 10–12 show another tendency that the farther from the inlet of the downer, the sharper the sudden fall of ozone concentration near the reactor wall. This indicates the lateral migration of solid particles from the downer centerline towards the wall when the flow of gas/solids suspension evolves from the acceleration stage into a fully developed stage. The solids concentration and slip velocity near the wall becomes higher over this process. As a result, the drop of concentration in the near wall region turns to be more obvious than before. The axial pressure distribution profile (e.g. Fig. 13) shows that the transition point (2 m below the inlet or $z/H = 0.23$) of pressure gradient (indicating the transition of flow regime [1]) is corresponding to the same axial position where a sharp concentration drop near the wall becomes obvious in the radial ozone concentration profiles. This indicates that the sharp drop near the wall region of ozone concentration profile is closely related to the change in flow patterns along the downer.

Another observation worth noting is the parabolic profile of ozone concentration near the entrance of the downer, which can be observed clearly, especially at higher gas velocities or solids circulating rates. The design of the entrance may account for this phenomenon, that is, the high speed jet of gas/solids mixed flow from the solids nozzle results in the non-uniformity mentioned above, and a higher superficial gas velocity can also accelerate the down-flow of the solids at the acceleration region of the downer (Qi et al. [25]).

3.3. Axial profiles of cross-sectional average ozone concentrations under different operating conditions

The axial profiles of ozone conversions are plotted in Fig. 14. It can be seen that most of the ozone was decomposed in the acceleration region, and the ozone concentration varied very little in the fully developed section (below $z/H = 0.29$) in the downer. This indicates that the reaction is much faster in the acceleration region than in the developed region because the higher solids concentration and reactant concentration there can increase the reaction rate of a first order reaction.

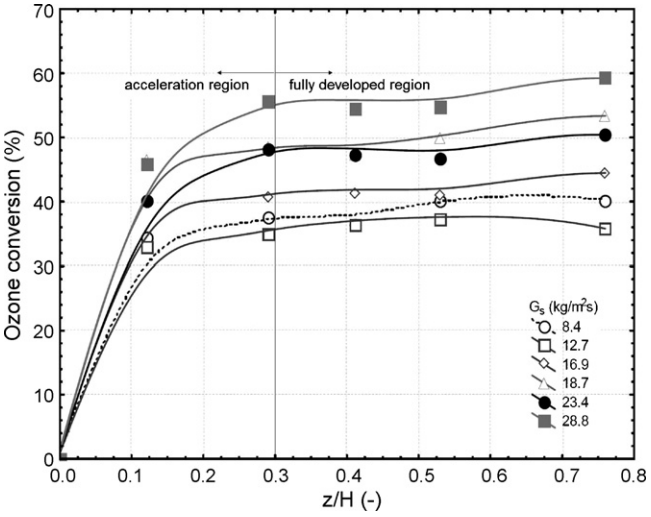

Fig. 14. Axial ozone conversion profiles for different values of G_s where $U_g = 2.6$ m/s.

In order to get an intuitionistic and visual depiction for the degree of ozone decomposition in the downer, the conversion of ozone at each axial position is plotted against operating parameters (superficial gas velocity and solids circulating rates) in Fig. 15 and Appendix D. The conversion increases mainly but with a little fluctuation along the direction of increasing G_s and decreasing U_g in the figure as illustrated before.

3.4. Mass transfer behavior in the downer

There are a lot of similarities between gas/solids mass transfer mechanisms of downer and riser. Therefore, based on works of Halder and Basu [26], mass transfer correlations for both units will have a similar form, such as

$$Sh = 2\varepsilon + A(Re/\varepsilon)^{B} Sc^{C}. \quad (1)$$

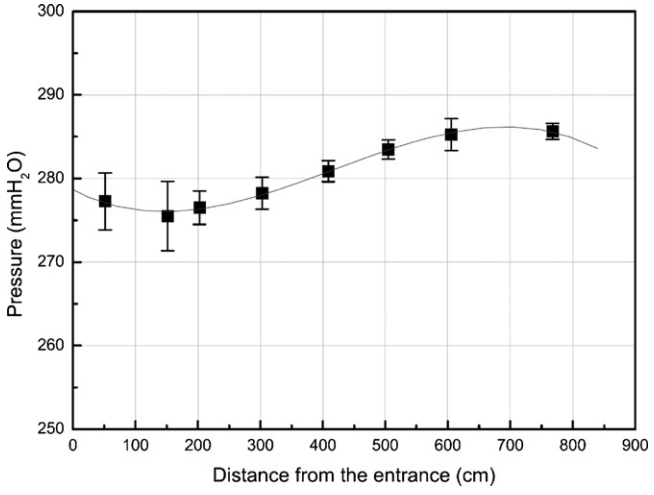

Fig. 13. An example of axial pressure distribution ($U_g = 3.1$ m/s, $G_s = 18.7$ kg/m^2 s).

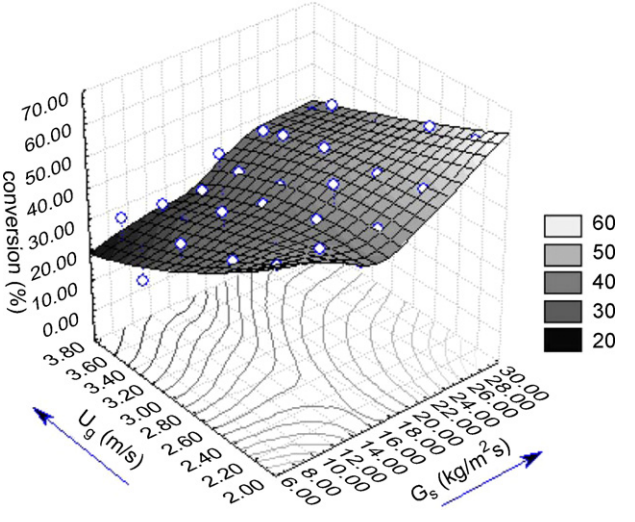

Fig. 15. Ozone conversion against operating parameters where $z/H = 0.53$.

where $Sh = k_g d_p/D_g$, $Re = d_p u_s/\nu_g$, $Sc = \nu_g/D_g$; A, B and C are parameters to be determined.

According to Eq. (1), the gas/solids mass transfer is composed of two parts, molecular diffusion(2ε) and convective mass transfer ($A(Re/\varepsilon)^B\ Sc^C$). In Eq. (1), k_g may be calculated from an infinitesimal mass balance for the downer; d_p is measured by the particle size analyzer; ν_g and D_g can be found or calculated from many reference handbooks; the slip velocity u_s between gas and particles can be evaluated on the basis of many previous researches [8,27]. Fitting part of the data from this experiment and some other experiments in the same downer, Zhang et al. [28] obtained a correlation shown below

$$Sh = 2\varepsilon + 0.0016\left(\frac{Re}{\varepsilon}\right)^{0.22} Sc^{0.57} \quad (2)$$

($2.49\ \text{m/s} < U_g < 4.15\ \text{m/s}; 2.77\ \text{kg/m}^2\ \text{s} < G_s < 12.21\ \text{kg/m}^2\ \text{s}$).

It is also found that the catalytic ozone decomposition in the downer is a mass transfer controlled process. This can be drawn from an ozone mass balance over an axial distance from z_1 to z_2 along the downer column [29]. The reduction of ozone in the downer is considered to be caused by the catalytic decomposition of ozone. That is,

$$U_g\ A_b(c_1 - c_2) = k[A_b(z_1 - z_2)]\ [\rho_p(1-\varepsilon)]c_s, \quad (3)$$

where A_b is the cross-sectional area of the downer column; ρ_p is the particle density; c_1, c_2, and c_s are the average ozone concentration at z_1, z_2, and particle surface; k is reaction rate constant; ε is the axial mean bed voidage calculated from pressure gradient.

Detailed calculation found that ozone concentration on the particle surface was much lower than that in the main gas flow (Fig. 16). So the gas/solid mass transfer may be the control step for the whole reaction process [30–32].

Compared the results with others' work [8,33], Zhang et al. [28] found that the local mass transfer at a given location in the downer (not the overall mass transfer) can be improved with increasing solids circulating rates and superficial gas velocity. In conclusion, much more systematic studies on the mass transfer characteristics in CFB downer reactor are still needed in the future for a comprehensive understanding of the whole reaction process.

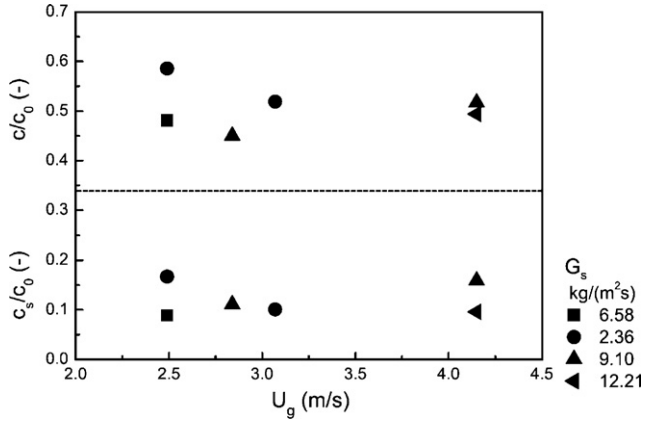

Fig. 16. Comparison of ozone concentration at particle surface and main gas flow.

4. Conclusions

The principal conclusions of the present research are as follows.

(1) The total amount of ozone decomposed in the downer increases with increasing solids circulating rate and decreasing superficial gas velocity. There is a compromise among several factors that leads to such a result, among which hydrodynamic behavior of clusters in the downer plays a key role.
(2) As noted by prior researchers, mass transfer is the main resistance for the gas/solids catalytic decomposition of ozone in the downer reactor, and increasing solids circulating rates or superficial gas velocity can improve local mass transfer behavior.
(3) Most of the ozone is decomposed in the acceleration region of the downer, which is thus important to the downer reactor, and more attention should be given to its design.
(4) The radial ozone concentration distribution in a downer is quite flat in the fully development region in the downer column, except for a very narrow region of $r/R = 0.8$–0.97 where there is a significant fall in the profile caused by faster reaction rate resulting from high concentration of catalyst due to solids segregating towards the wall region and falling faster than the dilute core region [23]. More significant sudden fall of the ozone concentration near the reactor wall corresponds to higher superficial gas velocities at a given solids circulating rate for the similar compromise mechanism. When the operating conditions are given, the ozone at this region in the fully developed section is decomposed more thoroughly than in the acceleration region due to the lateral particle migration during the flow regime transition process in the downer. More systematic and calibrated works should be devoted to the understanding of mass transfer in the near-wall region of the downer.

Acknowledgments

The financial supports from the National Natural Science Foundation of China (No. 20221603) and International Sci. & Tech. Cooperation Program of China (the Ministry of Science and Technology, PR China) (No. 2001CB711203) are gratefully acknowledged. Finally, special thanks to Prof. Mooson Kwauk for his valuable suggestions on this article.

Appendix A. Detailed description of experimental procedure listed in Fig. 5

Ozone from the ozone generator was first introduced into an absorption bottle filled with 20 wt.% KI solution along the path 1 for a certain period of time. Then the KI solution absorbed with ozone from the absorption bottle was acidized by dilute H_2SO_4 (1:5) solution before titrated by $Na_2S_2O_3$ (0.1000 mol/L a.q.) to determine the ozone concentration in the gas coming out from the ozone generator.

Next, the gas stream from the ozone generator was switched into gas path 2 and entered into the catalyst filled fixed bed reactor from the top. The outlet ozone concentration was measured by the same procedure as mentioned above by the iodimetry, with the gas flow rate being monitored by a wet gas flow meter. Mercury manometers were used to monitor the pressure fluctuation at the inlet and outlet of the fixed bed.

Before the reaction rate constant was calculated, the external dispersion and internal dispersion effect had been eliminated according to the method suggested in general chemical reaction engineering text books (i.e., varying the gas velocity or particle size under a particular contact time until no significant variation of conversion is observed) in order to assure the kinetic test could be performed under a proper gas velocity and particle diameter.

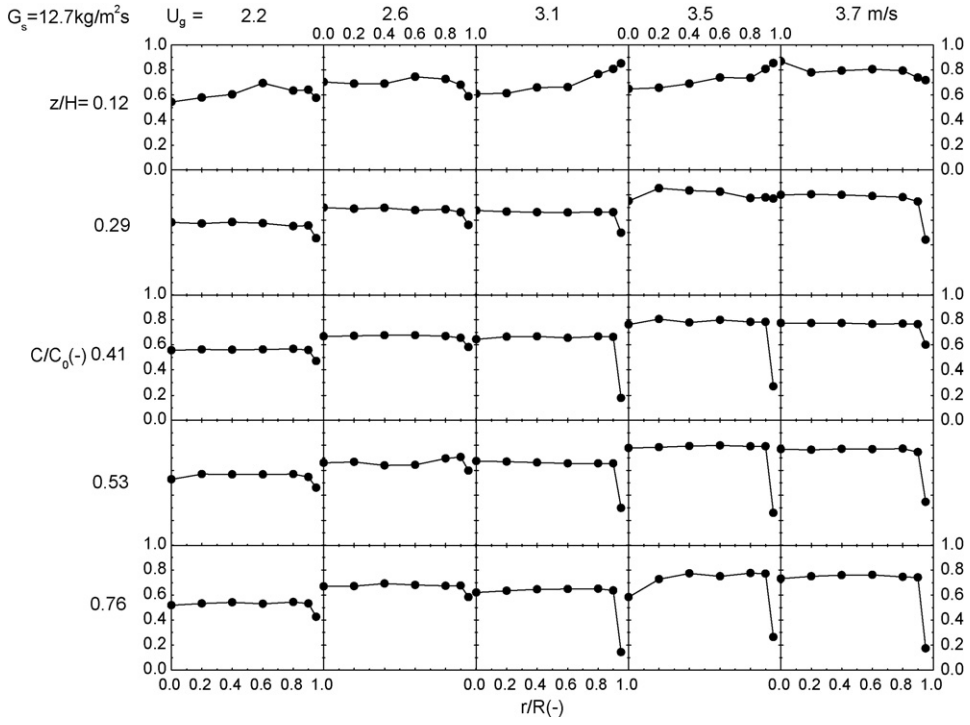

Fig. B1.

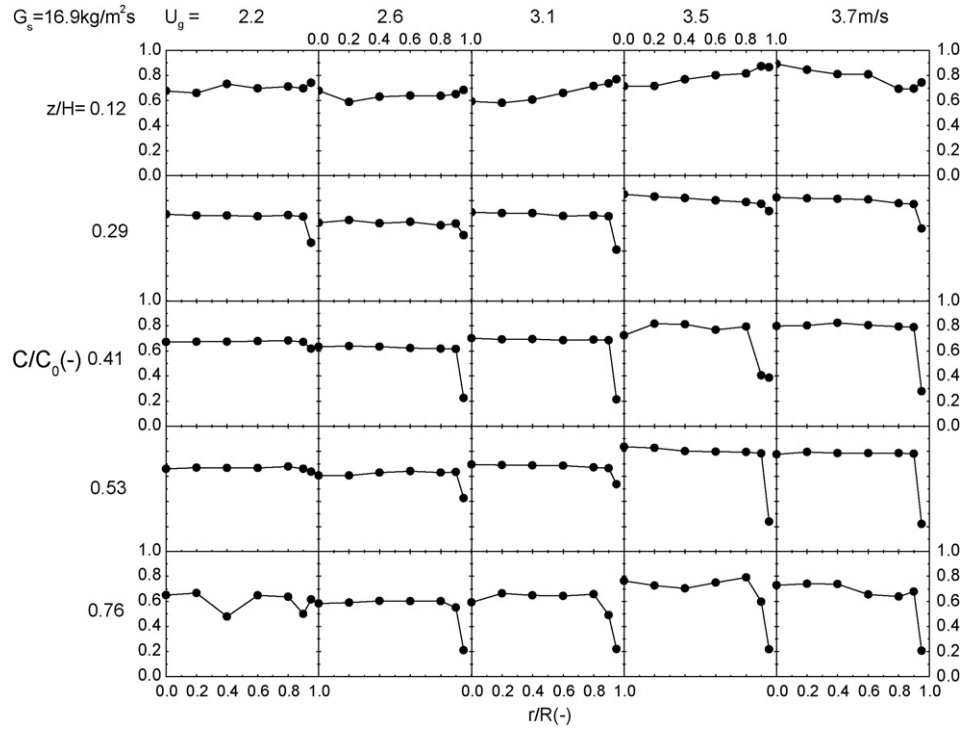

Fig. B2.

Appendix B

Additional figures of ozone distribution at various U_g under the same G_s (Figs. B1–B4)

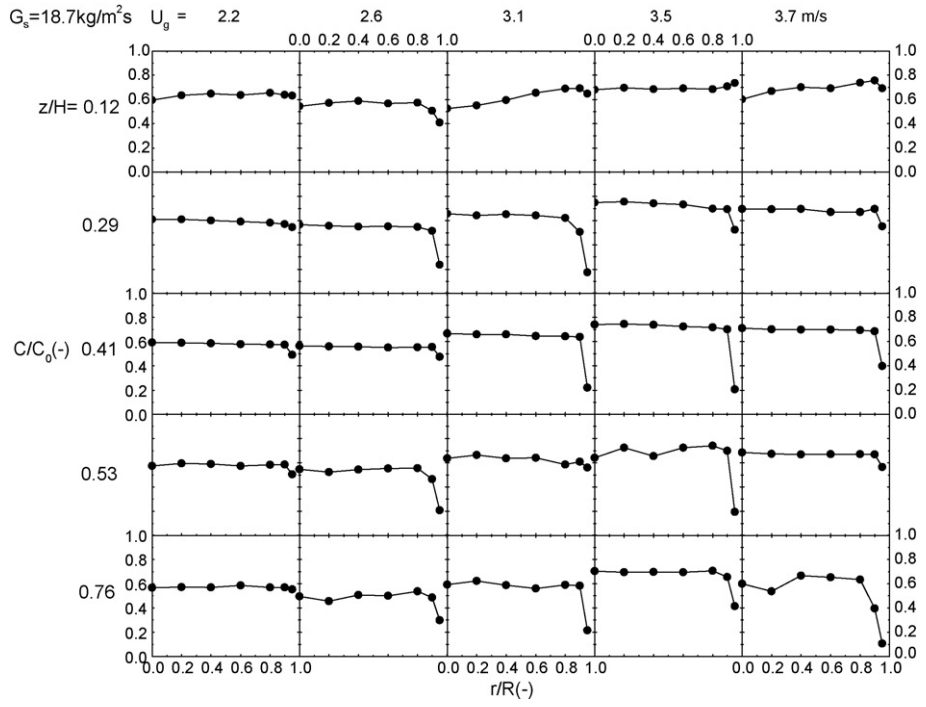

Fig. B3.

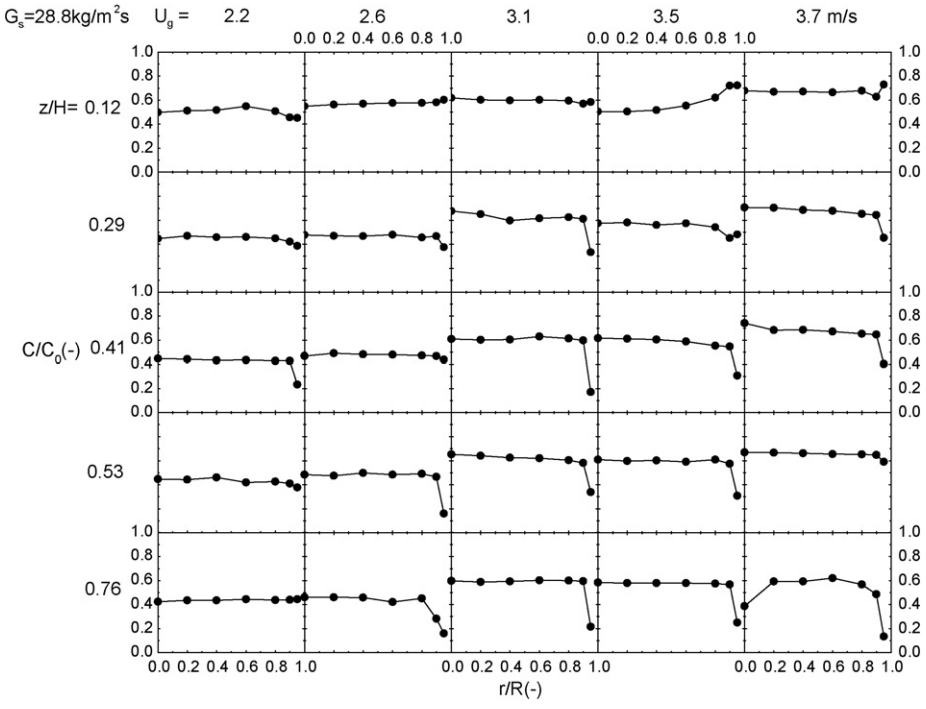

Fig. B4.

Appendix C

Additional figures of ozone distribution at various G_s under the same U_g (Figs. C1–C3)

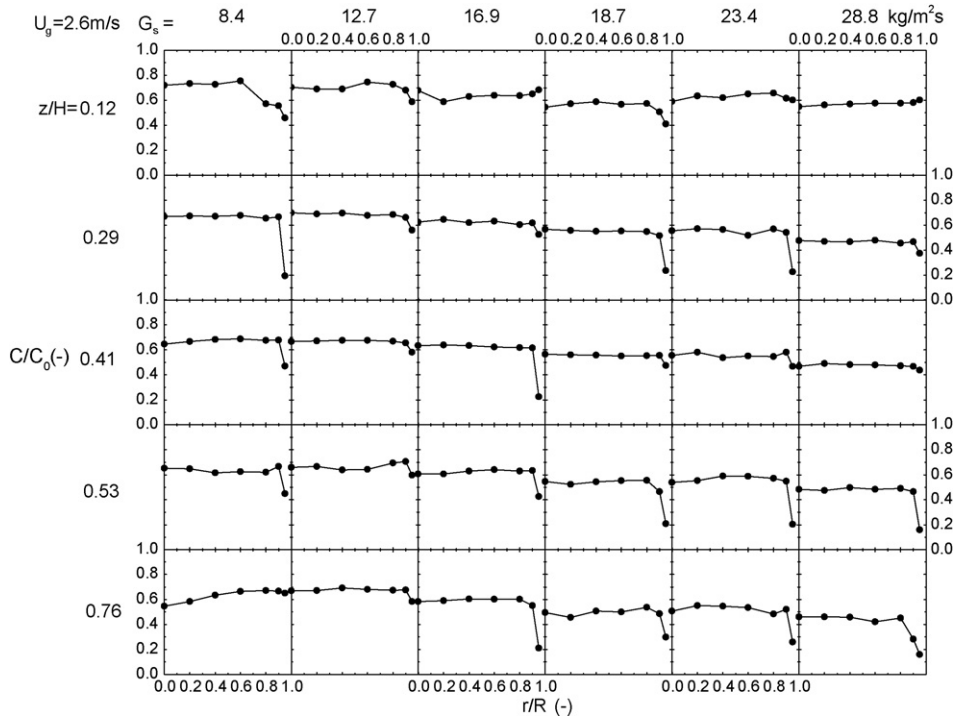

Fig. C1.

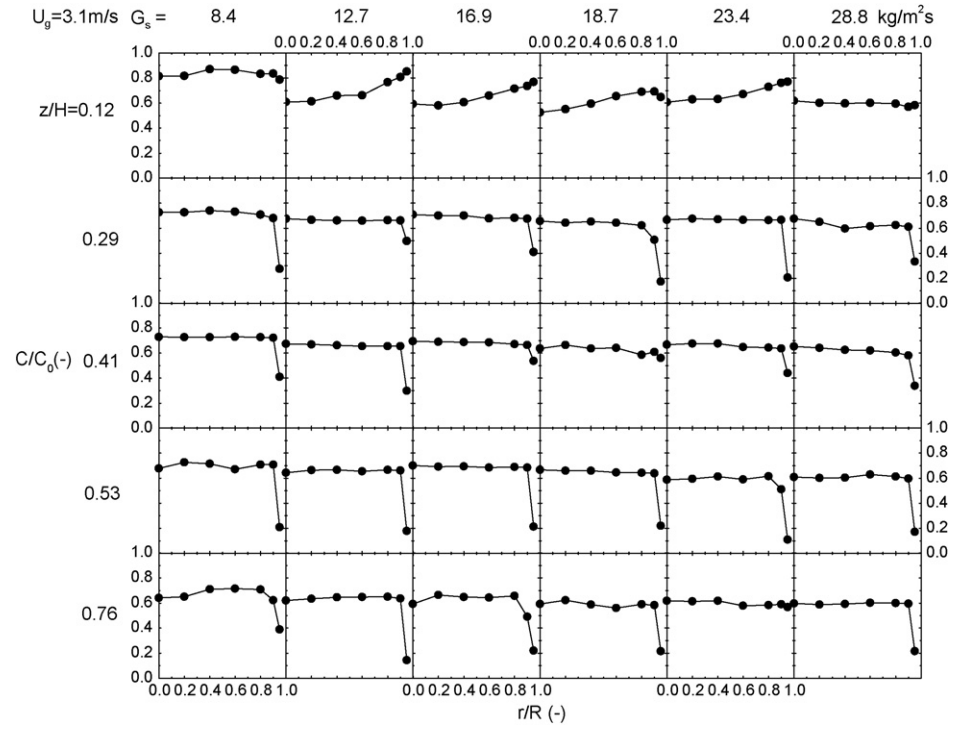

Fig. C2.

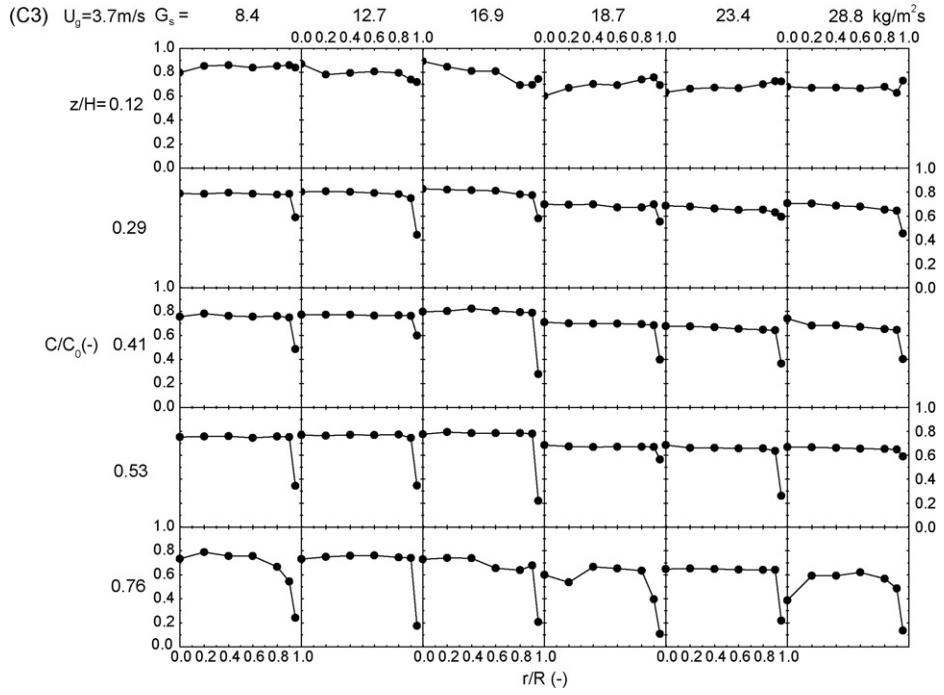

Fig. C3.

Appendix D

Additional ozone conversion against operating parameters at different axial locations (Fig. D1)

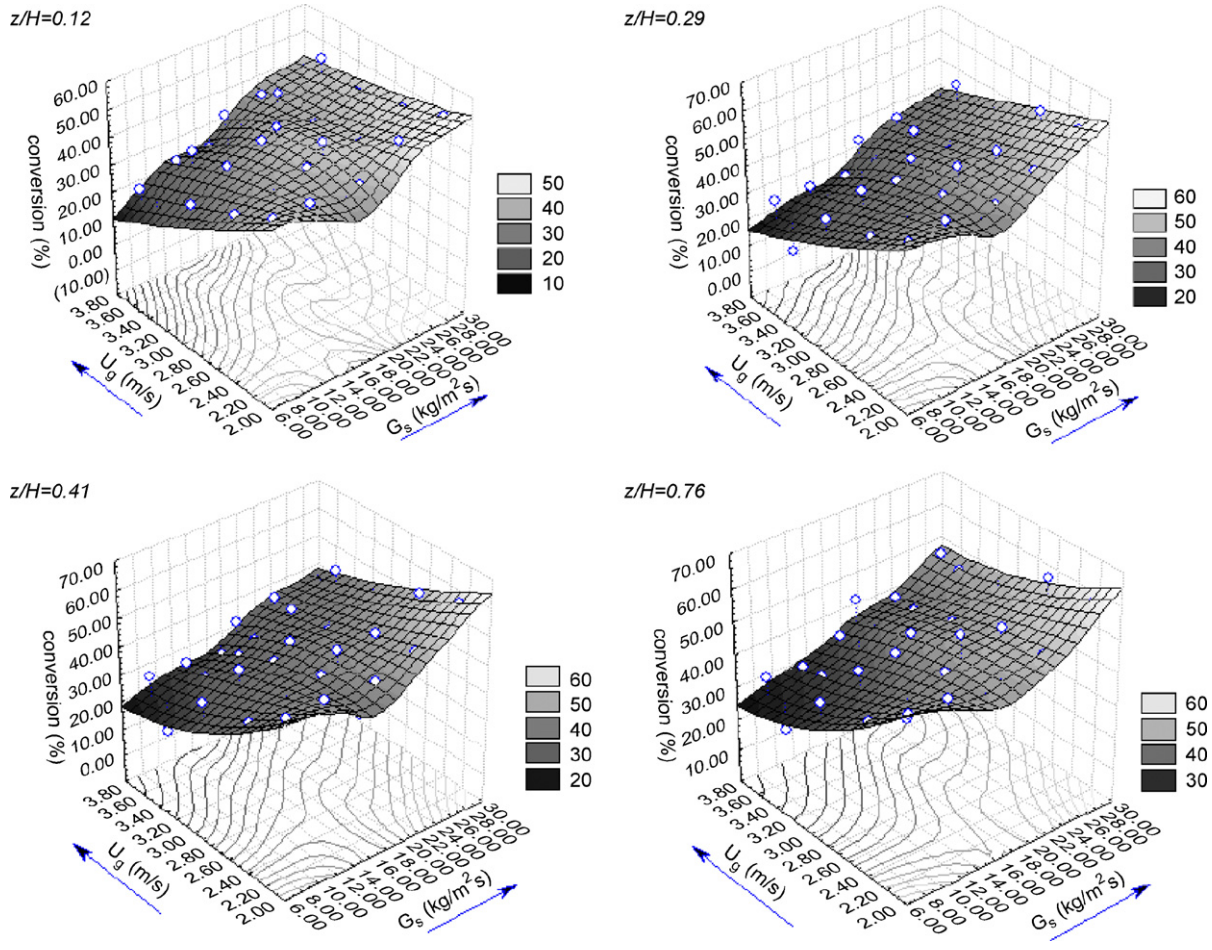

Fig. D1.

References

[1] J.-X. Zhu, et al., Can. J. Chem. Eng. 73 (1995) 662–677.
[2] T. Schiewe, et al., AIChE J. 45 (5) (1999) 949–955.
[3] H. Zhang, J.X. Zhu, M.A. Bergougnou, Chem. Eng. Sci. 54 (22) (1999) 5461–5470.
[4] M. Kwauk, Sci. Sin. 12 (4) (1963) 587–612.
[5] J.S. Ball, J.J.X. Zhu, Chem. Eng. Technol. 23 (8) (2000) 701–705.
[6] B. Wu, J.X. Zhu, L. Briens, Chem. Eng. Technol. 30 (4) (2007) 448–459.
[7] Y. Ma, J.-X. Zhu, Chem. Eng. Sci. 54 (54) (1999) 41–50.
[8] B. Luo, et al., Chem. Eng. J. 132 (1–3) (2007) 9–15.
[9] C.G. Frye, W.C. Lake, H.C. Eckstrom, AIChE J. 4 (4) (1958) 403–408.
[10] B.A. Partridge, P.N. Rowe, Trans. Int. Chem. Eng. 44 (1966) T335–T348.
[11] C. Fryer, O.E. Potter, AIChE J. 22 (1) (1976) 38–47.
[12] P. Jiang, et al., AIChE J. 37 (9) (1991) 1392–1400.
[13] S. Pagliolico, et al., Chem. Eng. Sci. 47 (9–11) (1992) 2269–2274.
[14] S. Ouyang, X.G. Li, O.E. Potter, AIChE J. 41 (6) (1995) 1534–1542.
[15] H. Schoenfelder, M. Kruse, J. Werther, AIChE J. 42 (7) (1996) 1875–1888.
[16] S. Ouyang, J. Lin, O.E. Potter, Powder Technol. 74 (1) (1993) 73–78.
[17] S. Li, W. Lin, J. Yao, Chin. J. Proc. Eng. 2 (1) (2002) 12–16.
[18] O. Bolland, Norwegian Univ. of Sci./Tech., Dept. of Thermal Energy and Hydropower, N-7034 Trondheim, NTNU, Norway, 1998, pp. 1–82.
[19] O. Bolland, R. Nicolai, in: H. Arastoopour (Ed.), Advanced Technologies for Fluid-Particle Systems, 1999, pp. 52–60.
[20] S. Li, Submitted to Institute of Process Engineering, Chinese Academy of Science, Graduate School of Chinese Academy of Science, Beijing, 2004.
[21] M. Zhang, et al., J. Chem. Ind. Eng. (China) 54 (2) (2003) 182–187.
[22] J. Zhu, F. Wei, Chem. React. Eng. Technol. (Chinese) 12 (3) (1996) 323–325.
[23] C. Cao, H. Weinstein, AIChE J. 46 (3) (2000) 515–522.
[24] M. Kruse, J. Werther, Chem. Eng. Proc. 34 (3) (1995) 185–203.
[25] C. Qi, et al., J. Chem. Ind. Eng. (China) 3 (1990) 273–280.
[26] P.K. Halder, P. Basu, AIChE, New York, NY, USA, New York, NY, USA, 1988, pp. 58–67.
[27] S. Li, W. Lin, J. Yao, China Particuol. 1 (6) (2003) 258–261.
[28] Y. Zhang, et al., Chin. J. Proc. Eng. 7 (1) (2007) 19–23.
[29] Y. Zhang, Institute of Process Engineering, Chinese Academy of Sciences, Beijing, 2006, p. 85.
[30] O. Levenspiel, Chemical Reaction Engineering (third ed.) [M], John Wiley & Sons, Inc., New York, 1999, pp. 368–472.
[31] S.-f. Li, Chemical and Catalytic Reaction Engineering, second ed., Chemical Industry Press, Beijing, 1986, in Chinese [M].
[32] L. Zhang, Z.-M. Xu, X.-Q. Yuan, in: Fundamentals of Chemical Reaction Engineering (in Chinese) [M], East China Univ. of Sci. & Technol. Press, Shang Hai, 2000, pp. 143–176.
[33] F. Wei, et al., Chem. Eng. Technol. 18 (1995) 59–62.